Polypropylene/Clay Nanocomposites: Combined Effects of Clay Treatment and Compatibilizer Polymers on the Structure and Properties

J. I. Velasco,[1] M. Ardanuy,[1] V. Realinho,[1] M. Antunes,[1] A. I. Fernández,[2] J. I. González-Peña,[3] M. A. Rodríguez-Pérez,[3] J. A. de Saja[3]

[1]*Centre Català del Plàstic, Departament de Ciència dels Materials i Enginyeria Metal·lúrgica, Universitat Politècnica de Catalunya, C/ Colom 114. E-08222 Terrassa (Barcelona), Spain*
[2]*Departament de Ciència dels Materials i Enginyeria Metal·lúrgica, Universitat de Barcelona, Martí i Franquès 1, E-08028 Barcelona, Spain*
[3]*Departamento de Física de la Materia Condensada, Cristalografía y Mineralogía, Facultad de Ciencias, Universidad de Valladolid, Prado de la Magdalena s/n, E-47011 Valladolid, Spain*

Received 14 December 2005; accepted 7 March 2006
DOI 10.1002/app.24419
Published online in Wiley InterScience (www.interscience.wiley.com).

ABSTRACT: Combined effects of clay treatment and compatibilizer polymers on the structure and properties of polypropylene/clay nanocomposites were studied. Dynamic mechanical analysis was used to analyze comparatively the dynamic mechanical response of different nanocomposites prepared from polypropylene and montmorillonite-rich bentonite, and to relate such response with the material microstructure. Two different bentonites were used: a purified Spanish natural bentonite was organophillized by means of 11-undecyl-ammonium ion and a commercial bentonite organophillized with dimethyl dehydrogenated tallow ammonium ion. Three different polar copolymers were employed as compatibilizer agents in some of the formulations: maleic anhydride-grafted polypropylene, maleic anhydride-grafted poly(styrene-*co*-ethylenebutylene-*co*-styrene), and poly(ethylene terephthalate-*co*-isophthalate) (PET). To ascertain the microstructure characteristics in the nanocomposites, wide angle X-ray diffraction, transmission electron microscopy, and differential scanning calorimetry techniques were used. The nanocomposites containing both bentonite organophillized with 11-undecyl-ammonium ion and PET, and maleated PP as compatibilizer system, were found to have the highest storage modulus and the smallest loss factor values, which was mainly due to the better clay platelets dispersion. The dynamic mechanical response of nanocomposites prepared with bentonite organophillized with dimethyl dehydrogenated tallow ammonium ion and maleated SEBS was strongly affected by the presence of this compatibilizer. The temperature of PP and α, β, and γ relaxations strongly depended on the interactions between the different phases in the nanocomposites. © 2006 Wiley Periodicals, Inc. J Appl Polym Sci 102: 1213–1223, 2006

Key words: nanocomposites; polypropylene; compatibilization; dynamic mechanical analysis (DMA)

INTRODUCTION

Scientific research on preparation and characterization of polymer/clay nanocomposites has grown continuously in the last few years with the general aim of developing new polymeric materials with improved characteristics.[1–16] Polypropylene (PP)/clay nanocomposites probably receive the highest interest because of the excellent ratio properties/cost of this polymer and its high versatility. Presently, PP nanocomposites find their greatest applications in the automobile, cable, and packaging industries.

Owing to the low polarity of PP, it is usually necessary to use compatibilizer agents to promote strong interactions between polymer and clay, which causes effective clay platelets dispersion within the polymer melt by shear or elongational forces during the mixing process.[1] In addition, it is also required to modify clay by means of exchanging the interlamellar metallic ions of the clay by organic ones (e.g., alkyl ammonium). The organophillized clay particles, thus obtained, display an expanded crystalline structure because of the higher free volume of the organic ions.[2] Kawasumi et al.[3] used maleic anhydride-modified PP oligomers as compatibilizers to prepare PP/clay nanocomposites by melt blending. The dispersion of the clay platelets was dependent on the miscibility of the maleic anhydride-modified PP oligomers in the PP matrix. Hasegawa et al.[4] reported an approach to prepare PP octadecyl amine-modified montmorillonite by using maleic anhydride-grafted polypropylene

Correspondence to: J. I. Velasco (jose.ignacio.velasco@upc.edu).

Contract grant sponsor: Spanish Ministry of Science (MEC); contract grant number: MAT2004-01563.

(MAH-*g*-PP) as compatibilizer. They found that silicate layers were partially exfoliated and dispersed to monolayers. Gloaguen and Lefebvre[5] prepared, by melt blending, a dispersion of organophilic clay in PP without compatibilizer, and they found evidences of polymer–clay platelet interaction, although no specific treatment was used to promote it. Nam et al.[6] prepared intercalated PP/clay hybrids by using a small amount of maleic anhydride groups as compatibilizer, to achieve disordered structures. Liu and Whu[7] reported the synthesis of intercalated PP/montmorillonite nanocomposites by grafting–melt compounding. Devaux et al.[8] reported how an *in situ* treatment of the clay by reactive processing may be a solution for avoiding the step of wet organophillization treatment of the clay. Polar acid/salt blends of ionomers and PA6 dispersed into molten PP were proposed. Moad et al.[9] reported a possibility of preparing PP/clay nanocomposites by direct melt-mixing using unmodified clays and a copolymer additive (1–3 wt %) based on a long chain acrylate. In the present article, compatibilized poly(ethylene terephthalate) (PET) combined with clay organophillization by means of undecyl ammonium ion is shown as an efficient way of clay platelet exfoliation into PP.

Otherwise, the dynamic mechanical response of PP/clay nanocomposites has been partially analyzed. Several papers[4,6,7,10–17] have considered the behavior of the storage modulus (E') and glass transition temperature (T_g). These works have shown that the addition of nanoclays increases the storage modulus. However, contradictory results were found with respect to the glass transition temperature; in most of these works, the T_g was practically unaffected by the presence of clays. In the PP nanocomposites,[13,16] the T_g shifted to high temperatures, whereas in Ref. 17 the T_g strongly shifted to lower temperatures. Several aspects of the dynamic behavior, such as loss factor values, the characteristics of α, β, and γ relaxations, and the activation energy of β relaxation, have not been analyzed in the former works. In the present article, the viscoelastic response of PP/clay nanocomposites is analyzed, through the effects induced by different clay organophillization treatments and compatibilizing polymers in the nanocomposite formulation.

EXPERIMENTAL

Materials

A fine high-purity bentonite fraction, rich in calcium montmorillonite (untreated clay), was obtained from bentonite (natural clay from Minas de Gador, Spain) and treated with undecyl ammonium chloride (UD-treated clay) according to a previously published procedure.[18] For a comparative study, we also used a commercial organoclay (Bentone 107, Elementis) consisting of bentonite rich in montmorillonite modified with dimethyl dehydrogenated tallow ammonium ion (DMDHT-treated clay).

Polypropylene (Isplen PP050) provided by Repsol-YPF (Puertollano, Spain) was used as polymer matrix. Poly(ethylene terephthalate-*co*-isophthalate) (PET) manufactured by Catalana de Polímers SL (El Prat de Llobregat, Spain) was used to investigate possible beneficial effects of PET presence on the characteristics of these nanocomposite materials. Eastman Chemical supplied a commercial grade of maleic anhydride-grafted polypropylene (MAH-*g*-PP) (Epolene G-3003), which was used as compatibilizer for the nanocomposites prepared with the UD-treated clay, while the compatibilizer used for the formulations prepared with DMDHT-treated clay was maleic anhydride-grafted poly[styrene-*b*-(ethylene-*co*-butylene)-*b*-styrene] triblock copolymer (MAH-*g*-SEBS) supplied by AK Elastomer (Tuftec M1913).

Nanocomposite preparation

PP/clay nanocomposites were prepared by a melt-compounding process performed in two stages. First, highly filled (typically 20 wt %) PP/clay composites were produced using a Collin ZK-35 corotating twin-screw extruder ($D = 25$ mm; $L/D = 36$). Intensive dispersive mixing was assured by means of various kneading blocks inserted in the screw configuration. A barrel temperature profile was selected from 150°C at the polymer feeding to 190°C at the end. Vacuum degassing was applied at a distance of 24 D from the feeding zone. The screw speed was fixed at 300 rpm. Under these conditions, the melt temperature measured at the die never exceeded 200°C. A circular cross section die of 3-mm diameter was employed, and the obtained extrudate was cooled in a water bath and pelletized. In a second extrusion process, performed under the same conditions, the clay concentration was reduced to a nominal percentage of 4 wt % by dilution with neat PP.

Seven different PP/clay nanocomposites were prepared (Table I). Two nanocomposites were based on a blend of PP and MAH-*g*-SEBS (90/10), containing 4 and 8 wt % of DMDHT-treated clay, called PP-CMMT-4 and PP-CMMT-8, respectively. A PP-based composite with no compatibilizer, containing untreated clay (called PP-MMT), was also prepared. In addition, PP-based composites with and without compatibilizer, containing UD-treated clay (PP-OMMT and PM-OMMT), and, two nanocomposites based on a compatibilized PP/PET blend containing untreated and UD-treated clay, respectively, were also prepared (BMP-MMT and BMP-OMMT).

Circular plates of 80 mm diameter and 3 mm thickness were compression-molded using a hot-plate press. The temperature was lower than 190°C and

TABLE I
Nominal Weight Compositions of the Nanocomposites Under Study

Sample	PP	MPP	PET	MSEBS	Untreated clay	UD-treated clay	DMDHT-treated clay
PP	100						
PP-CMMT-4	88			8			4
PP-CMMT-8	84			8			8
PP-MMT	96				4		
PP-OMMT	96					4	
PM-OMMT	94	2				4	
BMP-MMT	89	2	5		4		
BMP-OMMT	89	2	5			4	

the pressure 40 MPa. Prismatic specimens (25 × 4 × 3 mm^3) were machined from the discs to use in the dynamic mechanical analysis (DMA) experiments and in wide angle X-ray scattering (WAXS) and transmission electron microscopy (TEM) analysis.

Instrumental measurements

WAXS experiments were performed in a Siemens D-500 diffractometer using Cu Kα radiation (wavelength $\lambda = 0.154$ nm), operating at 40 kV and 30 mV. The step size was 0.05° (2θ) and the measuring time 5 s/step. The clay interlayer basal spacing (BS) was evaluated through the (001) reflection of montmorillonite.

Information about the nanocomposites morphology and microstructure was obtained from TEM. Ultramicrotomed sheets of 100–nm thick were used for the observations in a HITACHI H-800 microscope.

Differential scanning calorimetry measurements were performed using a Perkin–Elmer Pyris 7 calorimeter. Calibration of the instrument was done using standard samples of In and Pb. The sample mass was typically 10 mg. Once the sample thermal history was erased (for 4 min at 200°C), cooling cycles were conducted from 200 to 25°C, applying different cooling rates from 5 to 80°C/min. All runs were carried out in a stream of dried nitrogen. After each cooling, a heating run between 25 and 200°C was performed at 10°C/min. The crystallinity of PP was calculated according to the following equation:

$$X_m = \frac{\Delta H_m (m_c/m_p)}{\Delta H_0} 100 \tag{1}$$

where ΔH_m was the melting enthalpy measured in the heating experiments, ΔH_0 the theoretical enthalpy of PP 100% crystalline ($\Delta H_0 = 207.1$ J/g),[19] m_c the mass of the sample, and m_p the mass of PP in the sample.

Differences in the PP nucleation rate were evaluated through the activity parameter (ϕ) obtained from the method developed by Dobreva-Veleva and Gutzow.[20] The relationship proposed by these authors is the following:

$$\log q = \text{const} - \frac{B}{2.3\Delta T^2} \tag{2}$$

where q is the crystallization rate, ΔT is the undercooling ($T_m - T_c$), with T_m and T_c being the melting temperature and the peak crystallization temperature of the sample. The nucleation activity of the filler is related to the ϕ parameter.

$$\phi = \frac{B^*}{B^0} \tag{3}$$

B^* is the value of B when the polymer crystallizes in the presence of a nucleation agent, and B^0 when the nucleator is not present. The value of ϕ can decrease from 1 to 0, as the polymer nucleates in the presence of active substrates. This approach was successfully applied to evaluate nucleating rate differences of PP containing different mineral fillers.[21–24]

From the definition of B, the polymer crystal surface energy (σ) could be estimated:

$$B = \frac{16\pi\sigma^3 V_m^2}{3kT_m\Delta S_m^2 n} \tag{4}$$

And finally the lamella thickness (L), from the variant of the Gibbs–Thomson equation for a crystal of large lateral dimensions, and finite thickness was also estimated:

$$T_m = T_m^0\left[1 - \frac{2\sigma_e}{L\Delta H_m}\right] \tag{5}$$

In the aforementioned equations, k is the Boltzman's constant, T_m the PP melting temperature, ΔH_m the PP melting enthalpy, and σ_e is the specific surface energy. The PP molar volume (V_m) was taken equal to 28 cm^3/mol, the molar entropy (ΔS_m) 24.2 J/K, the Avrami exponent $n = 3$, and the melting temperature at equilibrium (T_m^0) 479 K.[23]

Dynamic mechanical thermal analysis (DMTA) testing was carried out using DMTA 7 Perkin–Elmer equipment, which was calibrated according to the standard procedure. The testing configuration was three-point bending with a support span of 20 mm. A static stress of 0.6 MPa and a dynamic one of ± 0.5 MPa were applied with a frequency of 1 Hz. For each specimen, two kinds of tests were performed. On one hand, dynamic loading was isothermally applied at 20°C to get quantitative results of the storage modulus (E') and the loss tangent (tan δ). The values were taken 5 min after applying the stresses, i.e., once the initial fluctuations of the values had disappeared. To ensure reproducibility, four measurements were registered for each material. On the other hand, the study of the secondary relaxations was carried out through tests performed in the temperature range from -40 to 130°C at a heating rate of 5°C/min. The glass transition temperature was determined as the temperature at the maximum in the loss modulus curve. T_α and T_γ were also determined in the loss modulus curves.

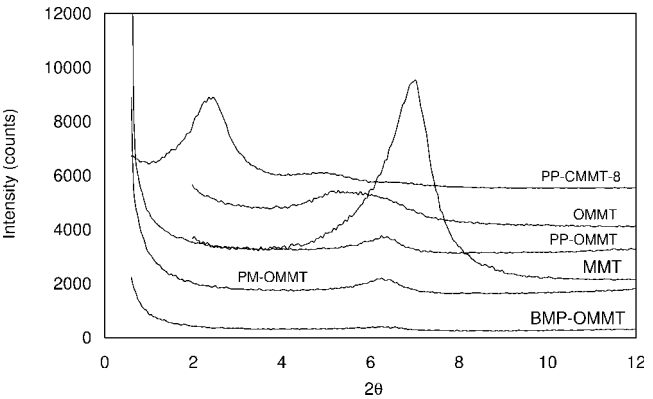

Figure 1 Comparative WAXS spectra of selected nanocomposites and bentonites.

Complementary measurements were carried out in DMA 861 METTLER equipment, with the testing configuration in the shear mode. Specimens of $5 \times 3 \times 3$ mm^3 were employed. A dynamic force of 16 N at variable frequency (1, 3, 5, and 10 Hz) was

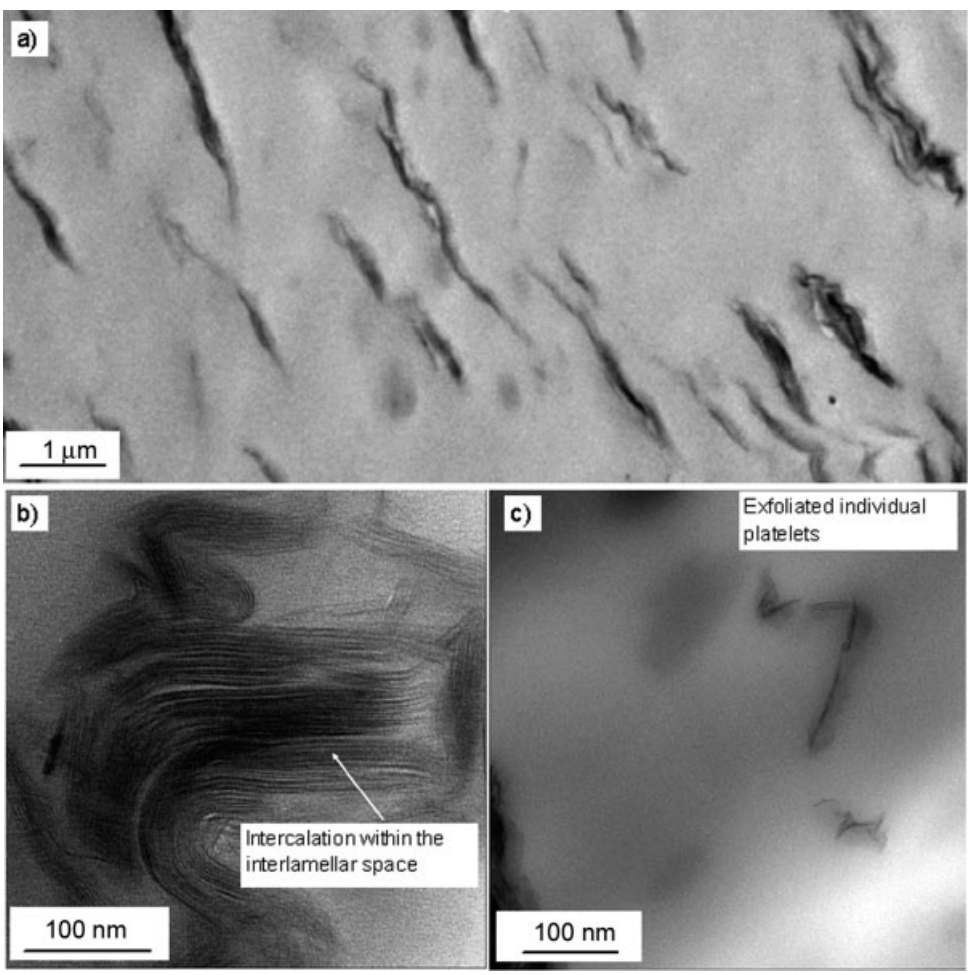

Figure 2 TEM micrographs of commercial DMDHT organoclay PP nanocomposites at different magnifications.

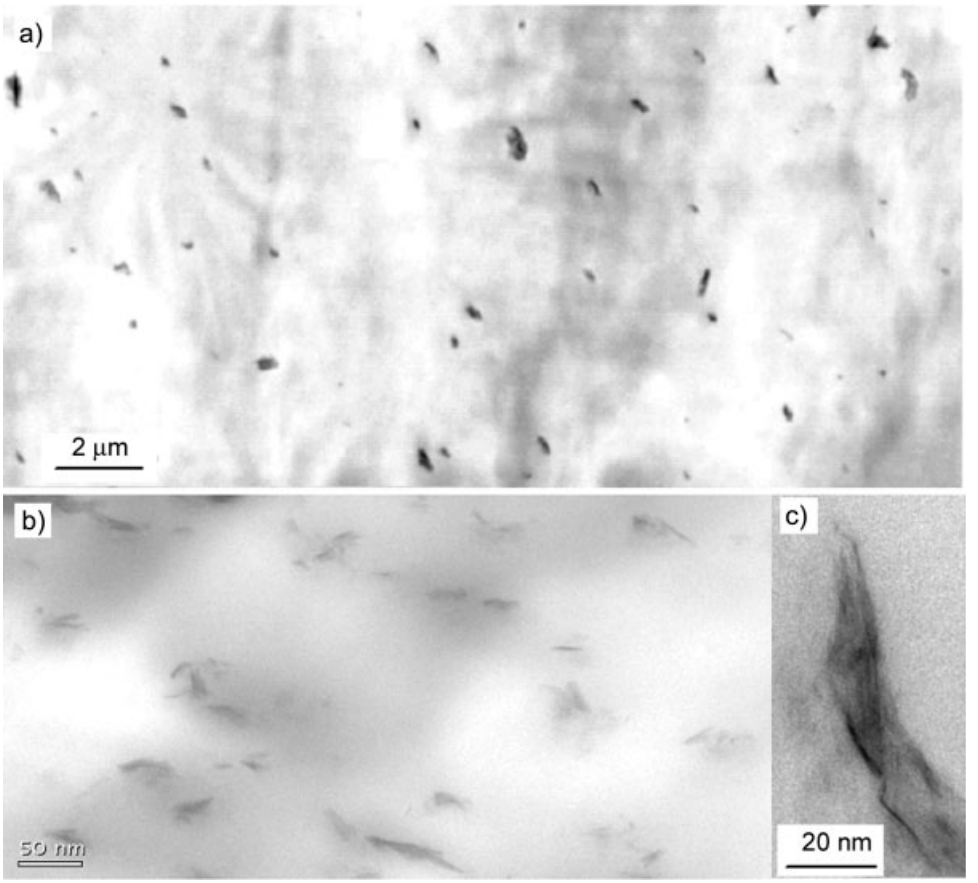

Figure 3 TEM micrographs of UD-treated clay PP nanocomposites (a) and UD-treated clay PP/PET nanocomposites (b and c).

applied in the range of temperature from −80 to 130°C, applying a heating rate of 5°C/min.

RESULTS AND DISCUSSION

Microstructure and morphology

The (001) reflection signal of both organoclays appeared in the WAXS patterns of the nanocomposites (Fig. 1), indicating that some extent of the crystal structure of the organoclay remained in the polymer matrix. Remarkable differences were found among the nanocomposites studied: in the nanocomposites containing the DMDHT-treated clay, the diffraction peak appeared at very low angles ($2\theta = 2.5^\circ$ for PP-CMMT-4 and $2\theta = 2.35^\circ$ for PP-CMMT-8), indicating a high structural expansion, $d_{(001)} = 3.53$ nm for PP-CMMT-4 and $d_{(001)} = 3.75$ nm for PP-CMMT-8, and consequently, facilitating the intercalation of macromolecular segments. In the nanocomposites containing the UD-treated clay, this signal appears at much higher angles (typically $2\theta = 6^\circ$), indicating much lower interlamellar expansion (typically $d_{(001)} = 1.7$ nm). Nevertheless, when the intensity of the (001) diffraction is analyzed, it may be observed that, for these nanocomposites, this intensity resulted considerably lower than in the nanocomposites with DMDHT-treated clay, mainly in BMP-OMMT nanocomposite, where the signal practically disappeared. A lower (001) diffraction signal intensity can be related to a higher extent of platelets exfoliation that occurred during the synthesis and processing of the nanocomposite. This hypothesis is supported by the TEM analysis. Figure 2(a) shows poor dispersion of DMDHT-treated clay particles in composites PP-CMMT-4 and PP-CMMT-8. The crystallites (tactoids) of this clay seem to be homogeneously distributed and oriented according the PP-melt flow direction. Despite the fact that, in these materials, the polymer intercalation within the interlamellar space of the DMDHT-treated clay resulted evident [Fig. 2(b)], only a few individual clay platelets were observed [Fig. 2(c)], mainly due to poor exfoliation. The nanocomposites containing the UD-treated clay show much finer clay particle dispersion by TEM [Fig. 3(a)]. Both, the smaller particle (tactoid) average size and the higher exfoliation degree were two remarkable differences of morphology between these nanocomposites. Furthermore, strong interaction between PET molecules and UD-treated clay would be expected to be due to the presence of

the carboxylic acid group of the undecyl ammonium exchanged montmorillonite (UD-treated clay). It was observed by TEM that PET encapsulated the clay platelets because of its high polarity [Fig. 3(b,c)].

Crystallization behavior

Results from the thermal analysis indicated that the bentonites would act as nucleation agents in the PP crystallization, as is revealed by the increase in the crystallization peak temperature [Fig. 4(a)], as well as the ϕ value reduction (Table II).

From the ϕ values, the PP nucleation rate increased as follows: PP + MSEBS < PP < PP-CMMT-4 < PP-CMMT-8 = PP-MMT < PM-OMMT < BMP-MMT < PP-OMMT < BMP-OMMT. Therefore, the organophillization of the bentonite with undecyl ammonium seemed to affect the PP nucleation activity (PP-MMT > PP-OMMT, and BMP-MMT > BMP-OMMT). Also, the nanocomposites prepared with UD-treated clay presented higher nucleation activity than did the nanocomposites prepared with the DMDHT-treated clay. As a consequence, both the surface energy and the theoretically calculated thickness values of the PP crystals were lower in the nanocomposites prepared with UD-treated clay than in the pure PP. Furthermore, the crystallinity degree was slightly higher than that of pure PP and remarkably higher than those of nanocomposites prepared with DMDHT-treated clay. A very high value of calculated PP lamella thickness also resulted in these latter nanocomposites. However, both effects can be explained as a result of the compatibilizer used in these nanocomposites, that is, because of the partial solubility of maleated SEBS into PP. In all the studied cases, the nucleation activity of the bentonites in PP was less effective than that displayed by other mineral fillers, like talc[21] ($\phi = 0.32$), magnesium hydroxide[22] ($\phi = 0.52$), or aluminum hydroxide[23] ($\phi = 0.54$).

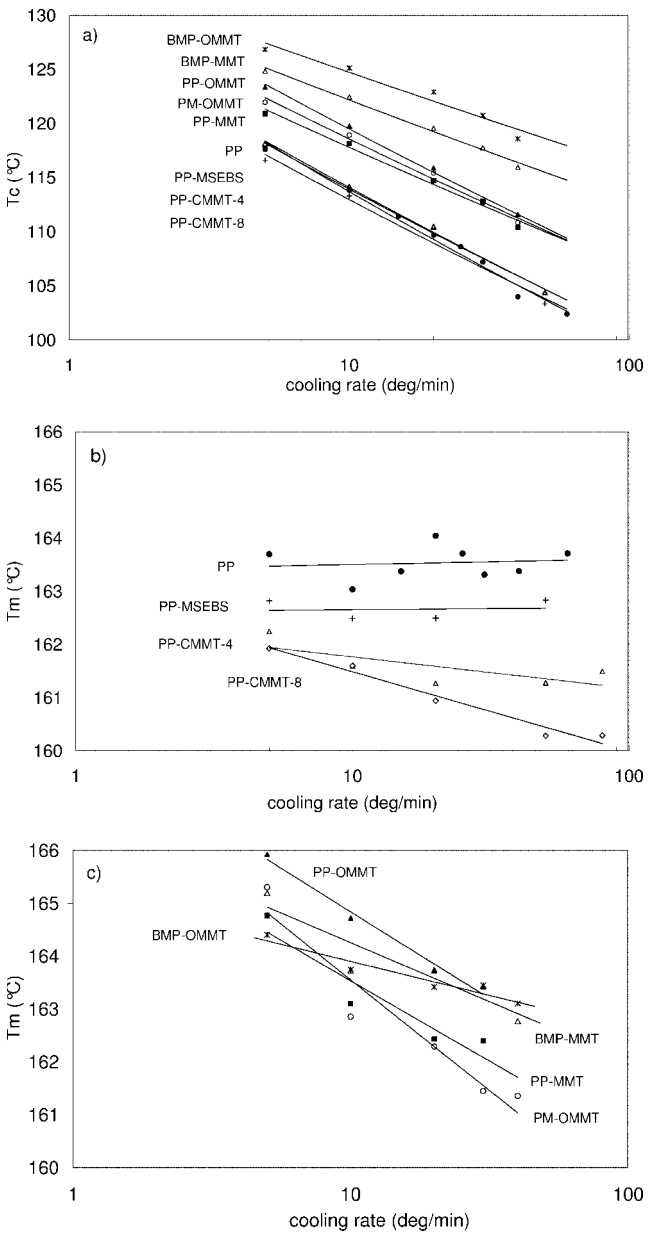

Figure 4 Crystallization (a) and melting peak temperatures (b and c) of PP versus the cooling rate.

The PET presence reinforced the nucleation activity of the clay in PP, leading to a reduction of the ϕ value in the composites based on PP/PET matrix, and particularly in the nanocomposites with organophillized clays. PET molecules not only would interact with UD-treated clay, but also with PP through the MAH functionality. These interactions could explain such increase of the nucleation activity. Similar behavior was previously observed in glass microsphere-filled PP composites.[24]

The stability of the PP crystal, in terms of the melting temperature versus the applied cooling rate, in the nanocomposites containing untreated and UD-treated clay, was lower than in the unfilled PP and DMDHT-treated clay composites, as can be concluded from the data of Fig. 4(b,c).

Dynamic–mechanical thermal behavior

Isothermal experiments

The storage modulus values obtained from isothermal experiments (Table III) showed that the presence of clay in the PP matrix increased the stiffness of the polymer. Moreover, in the nanocomposites containing both PET and UD-organophillized clay, this effect was more noticeable, showing that the better microstructure and finer morphology elucidated by WAXS and TEM resulted in materials with improved stiffness. This result could be ascribed to the high aspect ratio of clay platelets dispersed within the polymer matrix, as well as to the strong interactions between the matrix and the UD-treated clay.

TABLE II
Crystallization Characteristics Obtained by DSC

Sample	Average crystallinity,[a] X_m (%)	Activity parameter, ϕ	Crystal surface energy, σ (10^{-6} J/cm^2)	Lamellar thickness, L (10^{-9} m)
PP	54.1 (0.9)[b]	1.00	2.11	4.71
PP + MSEBS	41.1 (1.3)	1.11	2.19	7.13
PP-CMMT-4	46.4 (2.6)	0.95[c]	2.15	6.27
PP-CMMT-8	40.5 (1.5)	0.92[c]	2.12	6.99
PP-MMT	58.7 (3.2)	0.92	2.06	4.35
PP-OMMT	54.3 (2.4)	0.70	1.88	4.44
PM-OMMT	53.6 (4.5)	0.78	1.97	4.53
BMP-MMT	58.5 (2.4)	0.76	1.96	4.56
BMP-OMMT	55.6 (3.6)	0.69	1.90	4.63

[a] Average crystallinity values calculated from the melting endotherms obtained by heating at 10°C/min after crystallization at the different cooling rates.
[b] Values in parentheses indicate standard deviations.
[c] Values referred to the polymer matrix, polypropylene (PP) + maleated SEBS (MSEBS).

A decrease in the value of the loss factor with respect to the pure PP was observed when the UD-organophillized clay was present in the PP matrix. The presence of these organophillized clay platelets seemed to limit the molecular motions in the amorphous phase because of the interaction between the platelets and the PP matrix. On the contrary, the unmodified clay particles did not interact significantly with the polymer matrix; as a consequence, the molecular mobility in the amorphous phase was less limited and resulted in higher values of loss actor.

BMP-OMMT nanocomposites showed the lowest value of tan δ. Apart from the UD-treated clay's presence, such result can first be explained on a basis that, at room temperature, PET is under its glass transition temperature; therefore, a reduction of the viscoelastic character of the material is expected. Second, the presence of MAH-*g*-PP in the blend enhances the interfacial adhesion between phases, which would hinder the molecular motion of PP chains close to the interfaces, and thus the viscous dissipation phenomena would be constrained.

Similar to nanocomposites containing UD-treated clay, an increase in the storage modulus with respect to that of pure PP was observed for the nanocomposites prepared with DMDHT-organophillized clay and MAH-*g*-SEBS as compatibilizer. Nevertheless, the increase in E' value was less evident in these PP/CMMT nanocomposites, while the tan δ values was much higher than those of the other materials under study. The presence of MAH-*g*-SEBS would cause lower stiffness and higher molecular mobility, and consequently higher values of loss factor.

Dynamic experiments

McCrum et al.[25] reported that the dynamic loss modulus curve of PP exhibits three relaxations localized in the vicinity of −80°C (γ), 10°C (β), and 100°C (α). In crystalline polymers, the high-temperature (α) process is often related to the crystalline fraction, the β process is related to the amorphous phase, and in many cases is related to the glass transition, and the low-temperature (γ) process is generally considered to originate in the amorphous phase, but may also have

TABLE III
Storage Modulus (E') and Loss Factor (tan δ) Values from the Isothermal DMA Experiments; and Glass Transition (T_g), α′ Relaxation ($T_{\alpha'}$) and γ Relaxation (T_γ) Temperatures, as well as the Arrhenius Activation Energy (E_a) from the Nonisothermal DMA Shear Tests

Sample	E' (GPa)	tan δ	T_g (°C)	$T_{\alpha'}$ (°C)	E_a (kJ/mol)	T_γ (°C)
PP	1.02 (0.15)	0.0520	−0.5	52	411	−52
PP-CMMT-4	1.12 (0.05)	0.0656	−4.0	50	352	−46
PP-CMMT-8	1.20 (0.01)	0.0711	−4.0	42	348	−50
PP-MMT	1.20 (0.15)	0.0571	−6.5	–	318	−63
PP-OMMT	1.21 (0.06)	0.0439	−0.5	54	385	−63
PM-OMMT	1.18 (0.06)	0.0505	−0.5	57	297	−59
BMP-MMT	1.30 (0.10)	0.0474	−4.5	60	278	−52
BMP-OMMT	1.63 (0.14)	0.0436	−2.0	59	441	−56

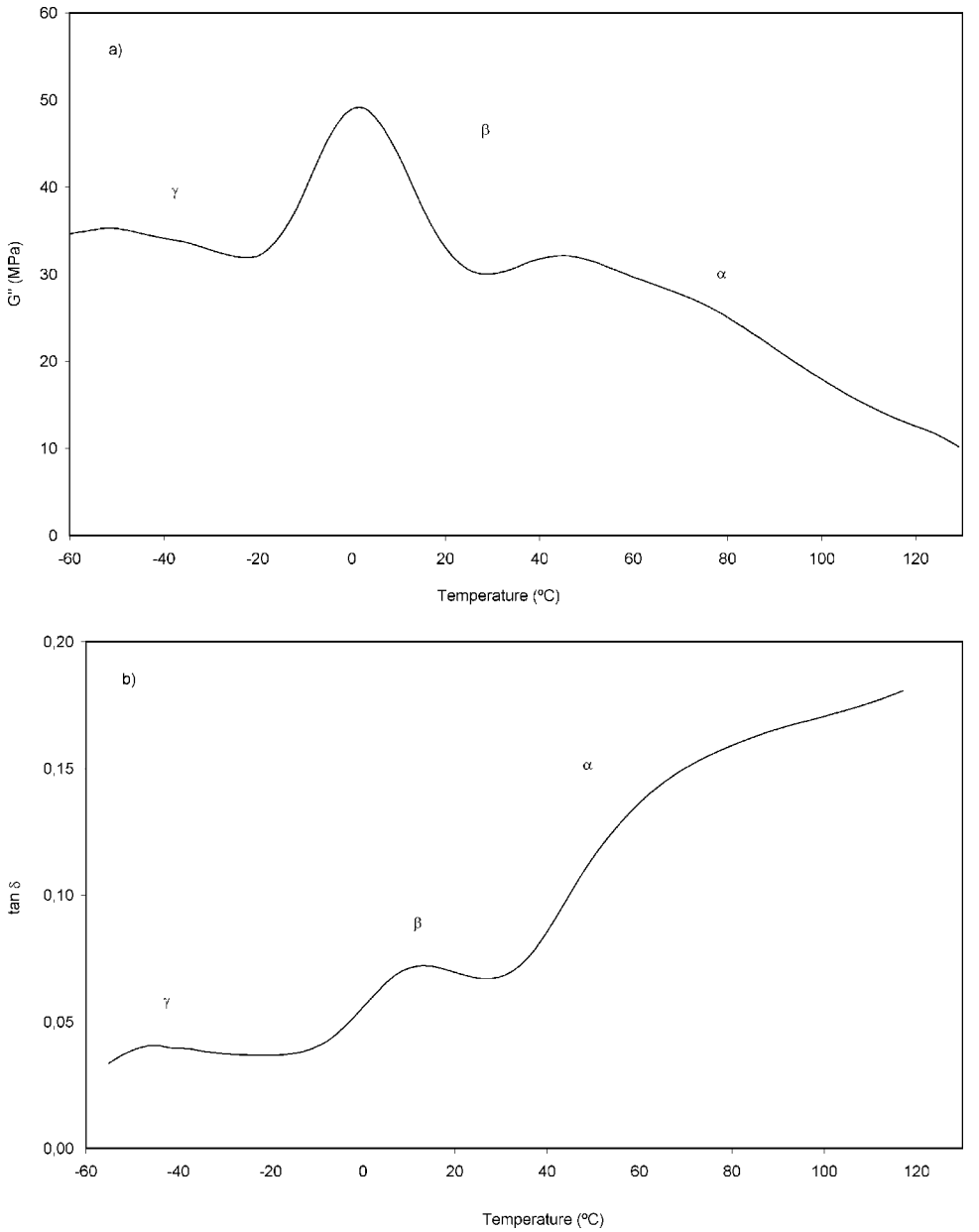

Figure 5 PP nanocomposites' thermal transitions observed in loss modulus and loss factor curves (BMP-MMT sample).

an important component associated with the crystalline phase.[26] The results for the PP nanocomposites displayed the three previous relaxations. Figure 5 is an example of the loss modulus and loss factor curves, showing the three relaxations.

The nanocomposite dynamic storage modulus is shown in Figure 6 as a function of temperature. In good agreement with isothermal results, both BMP-MMT and BMP-OMMT samples displayed the highest values of E' for all the temperature ranges [Fig. 6(b)].

Figure 7 displays the variation of the nanocomposite relative storage modulus (referred to that of neat PP) with the temperature and helps to elucidate the effects of both, the used organoclay and compatibilizer, on the E' modulus. Moreover, the increasing curves clearly show that the addition of the natural bentonite particles (UD-treated and untreated clays) into PP increases the stiffness at all temperatures, this increase being more elevate when the temperature is increased. This relative improvement of the stiffness with the temperature demonstrates the improvement of thermal stability given by the presence of clay particles in the PP matrix. This behavior that is previously observed[4,7,13,14] is related to the strong reinforcement effect of the clay particles above the glass transition temperature (when materials become soft). The presence of PET and the compatibilizer MAH-*g*-PP increases the stiffness, this increase being more significant with the presence of organophillized clay. This enhancement of E' is ascribed to the

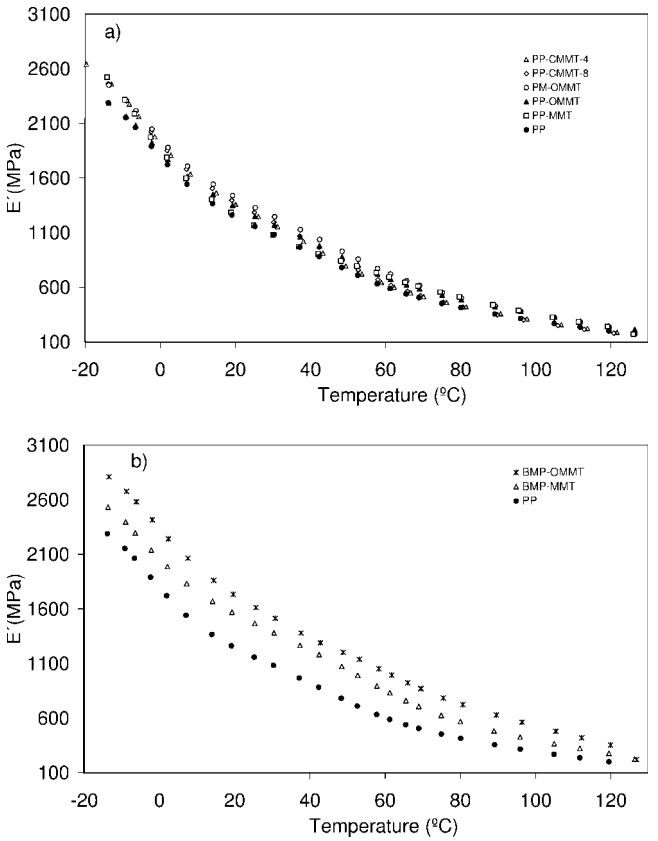

Figure 6 Experimental plots of storage modulus (E') versus temperature recorded by DMTA with three-point bending geometry.

better nanoscaled dispersion of these layered clays revealed by TEM and WAXS analysis, which resulted in higher aspect ratio in the reinforcing clay particles.

On the other hand, the MAH-*g*-SEBS presence combined with the DMDHT-treated clay seemed to have a contrary effect (decreasing curves in Fig. 7), probably due to the worse nanostructure achieved in these nanocomposites and to the higher mobility phase promoted by this compatibilizer.

The loss moduli (E'') of all the materials studied displayed a maxima at around 0°C, related with the β transition, which corresponds to the glass transition temperature of PP. The obtained values of the glass transition can be seen in Table III. As a general trend, the presence of the clays shifted T_g values to lower temperatures, mainly with unmodified clays. The smallest values were displayed by the PP-MMT and BMP-MMT samples. Higher values were found when the organophillized clays were mixed with the PP matrix. Once again, these results should be understood in terms of the reduced mobility of the polymer molecular segments and related to a higher interaction degree between the matrix and particle.

As mentioned in the Introduction, contradictory results have been observed relating the influence of the clay particles on the PP glass transition. Despite previous studies on conventional mineral-filled polymers, where adding a filler resulted in higher glass transition temperature, the results presented here have shown that, in the case of PP/clay nanocomposites, the glass transition occurred at similar or lower temperatures than for the pure PP. The same result has also been observed in talc-filled PP composites.[27] Different effects would affect the glass transition of PP/clay nanocomposites. So, with respect to the clay organophillization effect, higher interactions among the organophillized clay particles and the PP molecules would be the main reason for the differences found among the untreated and the organophillized clay nanocomposites. In the case of PP-MMT sample, the combined effects of not using compatibilizer and unmodified clay resulted in the lowest value of T_g (−6.5°C). Also, the low T_g value (−4.0°C) of PP-CMMT-4 and PP-CMMT-8 nanocomposites could be explained, despite the fact that they were prepared with an organophillized clay, with the basis on the presence of MAH-*g*-SEBS that provides high molecular motion to the amorphous phase.

From the loss modulus values obtained at various measuring frequencies, the apparent activation energy of the PP glass transition was calculated using the Arrhenius equation:

$$\frac{d[\ln(f)]}{d(1/T_p)} = -\frac{\Delta E}{R} \tag{6}$$

where f indicates the frequency of the experiments, and T_p corresponds to the T_g measured in the peak of the loss modulus curve. R is the gas constant and ΔE is the activation energy.

In general, the obtained activation energy values (Table III) show that this parameter is reduced in the nanocomposites with respect to pure PP. In addition, the ΔE values follow a general decreasing trend versus the glass transition temperature.

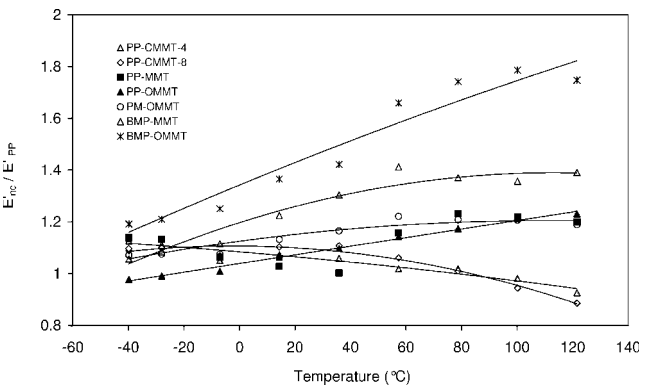

Figure 7 Evolution of the relative storage modulus of the nanocomposites with the temperature.

Concerning the PP α-relaxation, it was found that both the temperature and intensity of this relaxation were affected by the composition of the different nanocomposite materials. Both PP and PP/MAH-*g*-PP blend-matrix nanocomposites displayed similar intensity and peak position to pure PP, while in PP/MAH-*g*-PP/PET blends T_α values shifted to higher temperatures, the relaxation being more intense (Fig. 8). Similar results were found in PP/MAH-*g*-PP/PET blends filled with solid glass microspheres,[28] where this relaxation was also found to be very sensitive to the polymer thermal history. As can be seen in Figure 8(a), nanocomposites prepared with both DMDHT-treated clay and MAH-*g*-SEBS displayed lower T_α intensity and peak position. Therefore, the α relaxation is strongly affected by the interactions between PP and other phases in the material, increasing its intensity and shifting to higher temperatures when a compatibilized PP/PET blend is used as matrix, and decreasing its intensity and shifting to lower temperatures if MAH-*g*-SEBS is the compatibilizer.

The γ relaxation appeared at different temperatures (Table III) for the various nanocomposites. Different effects were observed. First, when only untreated clay particles were added to PP, the γ relaxation temperature strongly decreased (from −52.2 to −63°C). Second, this effect was less noticeable when MAH-*g*-PP or PET were used in nanocomposite formulation. Finally, these results were opposite in the case of PP-CMMT-4 and PP-CMMT-8 nanocomposites, which displayed the highest T_γ values, even higher than that of pure PP. Therefore, the three different compatibilizing polymers compensate in different extents the decrease of T_γ caused by the presence of the clay particles.

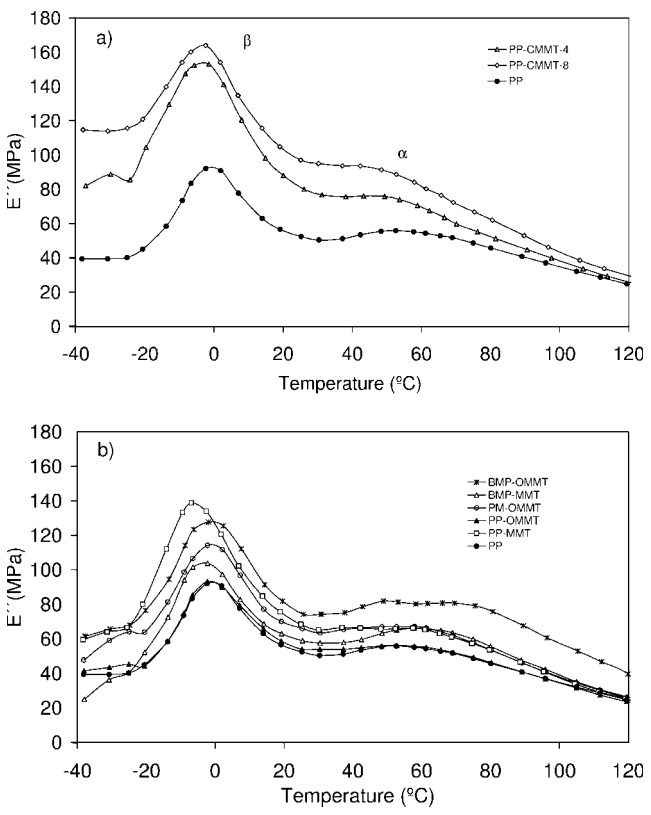

Figure 8 Loss modulus versus temperature curves.

CONCLUSIONS

The combined effects of clay modification and the type of polymeric compatibilizer on PP-matrix nanocomposites have been studied, focusing on the microstructure and dynamic mechanical response.

The clay organophillization treatment by means of a ''short'' (undecyl ammonium) ion resulted in lower basal interplanar distance increase than the ''long'' (DMDHT) ion-treated commercial clay. Nevertheless, the undecyl ammonium-treated bentonite, particularly when combined with compatibilized PP/PET blend, was successful for platelet exfoliation despite the low basal interplanar distance.

The PP storage modulus increased with the addition of clay particles, and this increase was higher when the organophillized clay was dispersed into the compatibilized PP/PET matrix, whereas the loss factor followed the opposite tendency. The better exfoliated microstructure, achieved for the PP/PET blend-matrix nanocomposites with MAH-*g*-PP as compatibilizer, resulted in the best improved dynamic–mechanical properties.

The organophillization of the clays reduced the PP glass transition temperature. It was observed that the PP α-relaxation appears at temperatures in the range of 40–60°C, its intensity being stronger and its peak temperature higher for the nanocomposites containing PET compatibilized with MAH-*g*-PP and lower for the nanocomposites with MAH-*g*-SEBS. It has also been observed that the PP γ-relaxation can be shifted to lower or higher temperatures, depending on the molecular mobility induced by the compatibilizer polymer.

References

1. Giannelis, E. P. Adv Mater 1996, 8, 29.
2. Oya, A. In Polymer-Clay Nanocomposites; Pinnavaia, T. J., Beall, G. W., Eds.; Wiley: Chichester, 2000; pp 151–172.
3. Kawasumi, M.; Hasegawa, N.; Kato, M.; Usuki, A.; Okada, A. Macromolecules 1997, 30, 6333.
4. Hasegawa, N.; Okamoto, H.; Kato, M.; Usuki, A. J Appl Polym Sci 2000, 78, 1918.
5. Gloaguen, J. M.; Lefebvre, J. M. Polymer 2001, 42, 5841.
6. Nam, P. H.; Maiti, P.; Okamoto, M.; Kotaka, T.; Hasegawa, N.; Usuki, A. Polymer 2001, 42, 9633.
7. Liu, X.; Whu, Q. Polymer 2001, 42, 10013.
8. Devaux, J.; Sclavons, M.; Fedullo, N. In Proceedings of 8th European Symposium on Polymer Blends and Eurofillers 2005; IUPAC: Bruges, 2005; F/262.

9. Moad, G.; Dean, K.; Edmond, L.; Kukaleva, N.; Li, G.; Mayadunne, R. T. A.; Pfaendner, R.; Rizzardo, E.; Simon, G.; Wermter, H. In Proceedings of 8th European Symposium on Polymer Blends and Eurofillers 2005; IUPAC: Bruges, 2005; F/195.
10. Wang, Y.; Chen, F. B.; Wu, K. C. J Appl Polym Sci 2004, 93, 100.
11. Gorrasi, G.; Tortora, M.; Vittoria, V.; Kaempfer, D.; Mülhaupt, R. Polymer 2003, 44, 3679.
12. Tjong, S. C.; Meng, Y. Z.; Hay, A. S. Chem Mater 2002, 14, 44.
13. Ma, J.; Qi, Z.; Hu, Y. J Appl Polym Sci 2001, 82, 3611.
14. Kim, J. H.; Koo, C. M.; Choi, Y. S.; Wang, K. H.; Chung, I. J. Polymer 2004, 45, 7719.
15. Chiu, F. C.; Lai, S. M.; Chen, J. W.; Chu, P. H. J Polym Sci Part B: Polym Phys 2004, 42, 4139.
16. Zhang, Y. Q.; Lee, J. H.; Jang, H. J.; Nah, C. W. Compos B Eng 2004, 35, 133.
17. Ding, C.; Jia, D.; He, H.; Guo, B.; Hong, H. Polym Test 2005, 24, 94.
18. Velasco, J. I.; Ardanuy, M.; Miralles, L.; Ortiz, S.; Maspoch, M. L.; Sánchez-Soto, M.; Santana, O. Macromol Symp 2005, 221, 63.
19. Wunderlich, B. Thermal Analysis; Academic Press: New York, 1990.
20. Dobreva-Veleva, A.; Gutzow, I. J Non-Cryst Solids 1993, 162, 13.
21. Alonso, M.; Velasco, J. I.; De Saja, J. A. Eur Polym J 1997, 33, 255.
22. Velasco, J. I.; Morhain, C.; Martínez, A. B.; Rodríguez-Pérez, M. A.; De Saja, J. A. Macromol Mater Eng 2001, 286, 719.
23. Velasco, J. I.; Morhain, C.; Martínez, A. B.; Rodríguez-Pérez, M. A.; De Saja, J. A. Polymer 2002, 43, 6813.
24. Arencón, D.; Velasco, J. I.; Rodríguez-Pérez, M. A.; De Saja, J. A. J Appl Polym Sci 2004, 94, 1841.
25. McCrum, E.; Read, B. E.; Williams, G. An elastic and Dielectric Effects in Polymeric Solids; Wiley: London, 1967.
26. Turi, A. Thermal Characterization of Polymeric Materials, Vol. 1; Academic Press: New York, 1997.
27. Rodríguez-Pérez, M. A.; Vasiliev, T.; Dobreva-Veleva, A.; De Saja, J. A.; Gutzow, I.; Velasco, J. I. Macromol Symp 2001, 169, 137.
28. Rodríguez-Pérez, M. A.; Velasco, J. I.; González-Peña, J. I.; Ruiz-Herrero, J. L.; Arencón, D.; De Saja, J. A. Macromol Symp 2005, 221, 247.